ACS OMEGA

Open Access

http://pubs.acs.org/journal/acsodf

Article

Structures Formed by Particles with Shoulderlike Repulsive Interaction in Thin Systems

Ryo Muragishi and Masahide Sato*

Cite This: *ACS Omega* 2023, 8, 30450−30458

Read Online

ACCESS | Metrics & More | Article Recommendations | Supporting Information

ABSTRACT: When particles are constructed in thin systems between two parallel flat walls, structures that are not observed in bulk systems are created and the created structures change, depending on the width between the walls. In this study, the structures formed by particles constructed in thin systems were investigated through performing isothermal−isobaric Monte Carlo simulations, where the interaction between the particles is given by the hard-core square shoulder potential. By controlling the width of the shoulder-like repulsive interaction and the system width, several novel structures such as the connection of rhombuses and the square lattice of the (100) face of the body-centered cubic lattice were created.

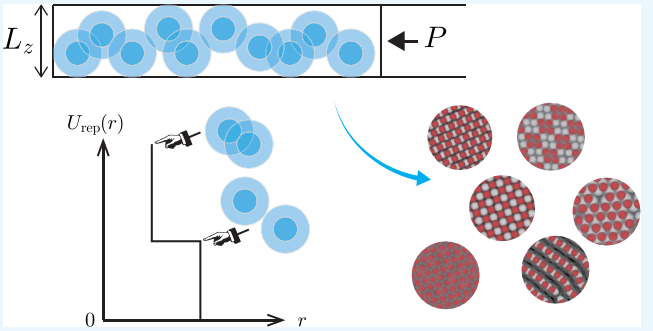

INTRODUCTION

Understanding the types of structures that form when particles are confined in a small space is important because structures that are not observed in bulk systems, such as square ice,[1] are created in small systems. For example, structures such as achiral packing phases and helical structures are created when particles are confined in cylindrical systems,[2,3] depending on the particle density and ratio of the radius of the cylindrical systems to the particle size. The difference in the structures affects the macroscopic mechanical, electrical, or optical properties of the materials.[4]

When particles are placed in a thin space between two parallel walls,[5−23] structures such as the face-centered cubic (FCC) structure, hexagonal close-packed structure, buckling structure, and prism phase are created, depending on the width between the walls, particle density, or pressure. In addition to the system size, system shape,[24−29] and particle shape,[26,30,31] the structures created in such small systems also depend on the interaction between particles.[15,18,21,32−35] The way in which structures are created in narrow systems has been investigated with consideration of many cases.

Recently, two-dimensional structures created by particles interacting with a hard-core square shoulder (HCSS) potential[36−44] has been investigated as structures created by a simple interaction potential. This potential is considered to be a potential simplified for systems such as microgel particles with a higher cross-link density,[45,46] rigid colloidal particles covered with a soft polymeric layer,[47−50] and block copolymer micelles consisting of a core of hydrophobic blocks surrounded by a shell of hydrophilic blocks.[51] Although the HCSS interaction potential is very simple, the formation of various structures depends on the pressure or particle density. When particles interacting with the HCSS potential are placed in a small container, they may create novel structures that have not been observed to date.[52]

By conducting isothermal−isobaric simulations, this study investigated structures created by particles interacting with the HCSS potential in thin systems between two parallel walls. Particularly, the types of the created structures and the dependence of the structures on the pressure, system, system width, and repulsive interaction width were investigated. The rest of this paper is structured as follows: first, the model used in the simulations is introduced. Then, the simulation results are presented and briefly discussed. Typical snapshots are shown, and by introducing some order parameters, average number of interacting particles, the radial distribution function, and the local rotational order are calculated. Finally, the simulation results are summarized.

METHODS

Potential. In the isothermal−isobaric Monte Carlo simulations conducted in this study, the HCSS potential[36−44] was used because it can create various two-dimensional structures even though it is a very simple procedure. The HCSS potential between the ith and jth particles, whose

Received: May 23, 2023
Accepted: July 25, 2023
Published: August 9, 2023

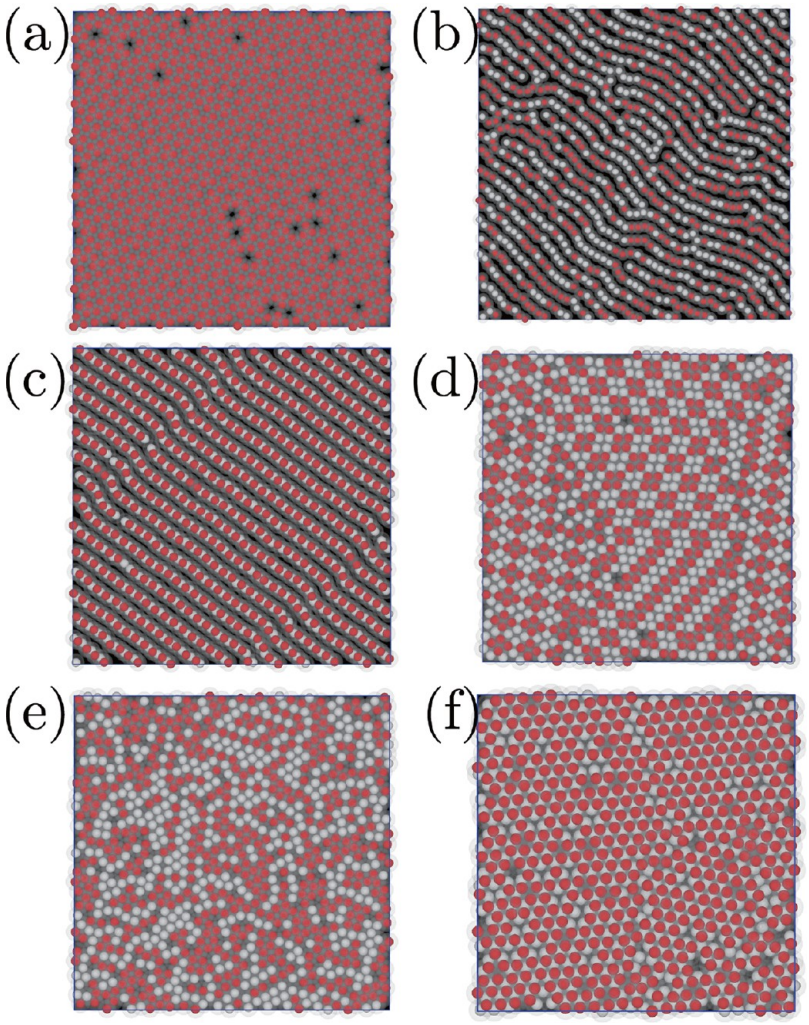

Figure 1. Snapshots viewed from the z-direction. δ is set to 2 σ, and L_z/σ and $P\sigma^3/k_BT$ are (a) 1 and 25, (b) 1.2 and 5, (c) 1.9 and 10, (d) 1.6 and 20, (e) 1.4 and 25, and f) 1.9 and 30. The particles in $z \geq L_z/2$ and $z < L_z/2$ are indicated by red and white spheres, respectively.

centers are located at $\boldsymbol{r}_i$ and $\boldsymbol{r}_j$, respectively, is expressed as follows:

$$U_{\mathrm{rep}}(r_{ij}) = \begin{cases} \infty & (r_{ij} < \sigma) \\ \epsilon & (\sigma < r_{ij} < \delta) \\ 0 & (\delta < r_{ij}) \end{cases} \quad (1)$$

where $r_{ij} = |\boldsymbol{r}_i - \boldsymbol{r}_j|$ is the distance between the center of the two particles and σ represents the diameter; ϵ and $\delta - \sigma$ are the strength and width of the shoulder-like repulsion, respectively. Simulations are conducted for several δ values with a ϵ / k_BT.

Initial Condition. Initially, the particles were randomly placed in a thin cuboidal system between two walls. The system volume is given by $L_x L_y L_z$, where L_x, L_y, and L_z are the system sizes in the x-, y-, and z-directions, respectively. The two walls were located at $z = 0$ and $z = L_z$. The wall positions were fixed, and L_x and L_y were changed during the simulations. Period boundary conditions were used in the x- and y-directions. The repulsion from the wall also affects the particle behaviors.[22] In this study, it was assumed that the particles are affected by repulsion from the walls when the distance between the walls and the particles is less than $\delta/2$. The strength of the repulsive interaction energy is given by ϵ and is similar to the repulsion between particles: the distance between the center of particles and wall cannot be smaller than $\sigma/2$

Isothermal−isobaric Monte Carlo simulations were conducted for systems with a particle number N of 1024. The repulsion strength ϵ was set to $5k_BT$, where k_B is the Boltzmann constant and T is temperature. The particle density ρ is given by $4\pi\ (\sigma/2)^3N/(3L_xL_yL_z)$. Initially, the particles were put in systems with $\rho = 0.15$. In these simulations, a change in the system volume was attempted after translation trials had been performed once for all the particles. During the change in the system volume, L_z was kept constant, while L_x and L_y were changed equally according to the pressure P. The trial sets of the volume change and the translation of the particle positions were carried out 10^7 times. To prevent the acceptance ratio of these trials from being too small, the maximum of translation value was tuned every 10 trials and the accept ratio of the trials was kept close to 0.5 during the simulations.

RESULTS AND DISCUSSION

Simulations were conducted with different L_z and P for several σ, and the types of structures were investigated. Initially, δ was set to 2.0σ because previous studies[39,41−44,52] have observed various structures when large δ was used. The dependence of

https://doi.org/10.1021/acsomega.3c03624
ACS Omega 2023, 8, 30450−30458

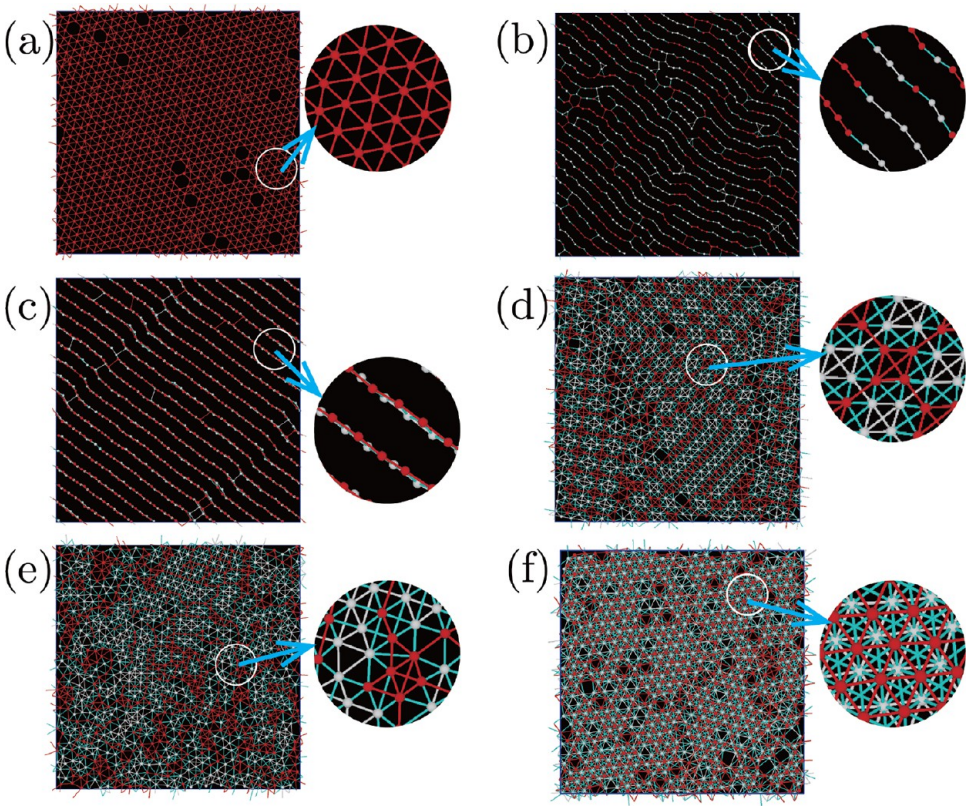

Figure 2. Snapshots of interactions viewed from z-direction for data used in Figure 1. δ is set to 2 σ, and L_z/σ and $P\sigma^3/k_BT$ are (a) 1 and 25, (b) 1.2 and 5, (c) 1.9 and 10, (d) 1.6 and 20, (e) 1.4 and 25, and (f) 1.9 and 30. The particles in $z \geq L_z/2$ and $z < L_z/2$ are indicated by small red and white spheres, respectively. The particles with repulsive interaction are connected with red lines when both particles are in the upper half region, white lines when both particles are in the lower half region, and blue lines when each particles are in a different region. Circular snapshots adjacent to Figure 2a–f are the snapshots zoomed in circular regions.

structures on $P\sigma^3/k_BT$ and L_z/σ was investigated for $P\sigma^3/k_BT$ = 5, 10, ⋯ , 25, 30 and L_z/σ = 1, 1.1, ⋯ , 1.9, 2. In these cases, the effect of shoulder repulsion on the formation of structures was neglected because the simulations were conducted for $\delta = 2.0\sigma$.

Snapshots for Typical Structures. Figure 1 shows snapshots of the typical structures observed in the simulations. The interacting particles are connected by lines in Figure 2, where the particles in $z \geq L_z/2$ and $z < L_z/2$ are indicated as small red and white spheres, respectively. When two particles are $z \geq L_z/2$, the particles are connected by red lines; when both particles are in $z < L_z/2$ are connected by white lines, the particles are connected by while lines; and when two particles are in different regions, the particles are connected by blue lines.

The structures and interactions between particles in Figure 2a,b are simple, but those in other cases are complicated. To show these structures more clearly, the interactions in Figure 2c–f are shown schematically in Figure 3i, ii, and iv. In addition to the schematic figure viewed from the z-direction, the interactions viewed from the horizontal direction are illustrated in Figure 3i because the lines overlap and the interactions are illegible in Figure 2c. Hereafter, each structure shown in Figure 2 will be described in detail.

Single-Layer Hexagonal Structure. For L_z/σ = 1 and $P\sigma^3/k_BT$ = 25 (Figure 1a), two-dimensional structures were created because the system width was as small as the particle diameter. Owing to the high pressure, a hexagonal structure, that is the (111) face of the FCC structure, was created but several voids existed. Because the lattice space is larger than σ, the hexagonal structure is a middle-density hexagonal lattice.[43] For a structure without voids, the number of interacting particles per particle, (N_B), is six, and the interaction energy per particle for creation of the structure is 3ϵ.

String-Like Structures. For L_z/σ = 1.2 and $P\sigma^3/k_BT$ = 5 (Figure 1b), a string-like structure is created. Because L_z is sufficiently small, the structure is a single-layer structure even though the z-coordinates of the particles in the structure fluctuate. As shown in Figure 2b, N_B is two and the interaction energy per particle for creation of the structure is ϵ. Because the pressure is lower than that in Figure 1a, N_B is smaller than that in Figure 1a. Thus, a structure with less repulsive interaction energy was created. In this string-like structure, the particles in $z \geq L_z/2$ and $z < L_z/2$ appeared at random because the structure became compact when the particle positions deviated in the z-direction.

When both L_z/σ and $P\sigma^3/k_BT$ increased, the particle arrangement in the string-like structure became regular and the strings were zigzag in the vertical direction. Particles with different z regions appeared alternately, as shown in Figure 1c. The strings arrayed regularly to prevent particles in different strings from interacting with each other in the structure (Figure 2c). Here, N_B is four, that is, each particle interacted with two particles in different z regions and two particles in the same z region, as shown in Figure 3i. Additionally, the interaction energy per particle for creation of the structure is 2ϵ, which is larger than that in Figure 1b.

Connection of Rhombic Tetramers. When $P\sigma^3/k_BT$ was sufficiently large and L_z is large to create double-layer

https://doi.org/10.1021/acsomega.3c03624
ACS Omega 2023, 8, 30450−30458

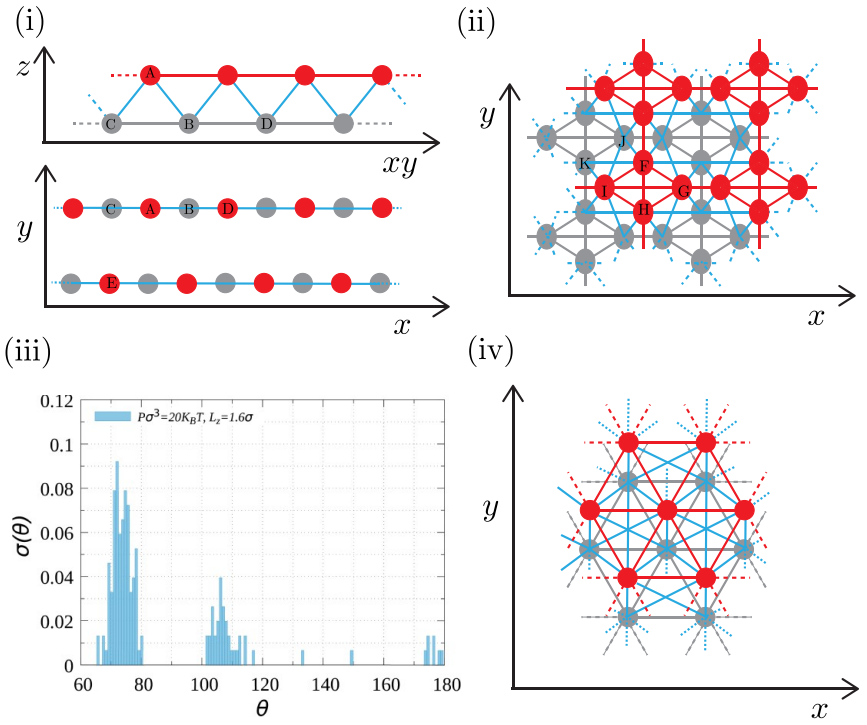

Figure 3. Schematics of typical interactions in (i) Figure 2c, (ii) Figure 2d, and (iv) Figure 2e. The particles in $z \geq L_z/2$ and $z < L_z/2$ are indicated by red and gray circles, respectively. Interacting particles are connected by a red line if both particles are in $z \geq L_z/2$ or a gray line if both particles are both in $z < L_z/2$. When the particles are in different regions, the particles are connected by a blue line. (iii) Distribution of angles for rhombic structures observed in Figure 2d.

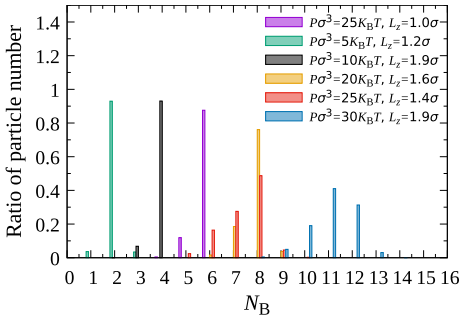

Figure 4. Distribution of N_B obtained from snapshots shown in Figure 1.

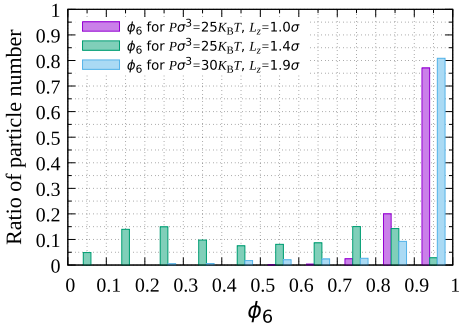

Figure 5. ϕ_6 for $(L_z/\sigma, P\sigma^3/k_BT)$ = (1, 25), (1.4, 25), and (1.9, 30), which were used for Figure 1a,e,f, respectively. For $(L_z/\sigma, P\sigma^3/k_BT)$= (1.4, 25) and (1.9, 30), ϕ_6 is calculated for particles in the same z-level.

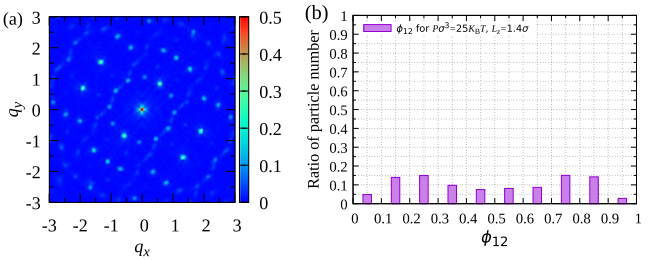

Figure 6. (a) $|S(q)|/|S(0)|$ and (b) local 12-fold local rotational order ϕ_{12} for Figure 1e.

structures, a more compact structure, such as Figure 1d, is created. As shown in Figure 3ii, this structure consisted of the double layers of the connection of the rhombic tetramers. Because the interaction between the particles shown in Figure 2d is more complicated compared with those in Figure 2a–c, to clarify the structure, the way in which the particles interacted with each other is shown in Figure 3ii. There are four types of particles, namely, F, G, H, and I. As shown by angle distribution for the rhombic tetramers (Figure 3iii), which was obtained by examining areas with many rhombic tetramers, the dominant angles are given by 70° and 110°. Thus, ∠FGH is 70° and ∠IFG is 110°. The distances between neighboring particles are different for these particles, but interacting energy per particle is the same for the particles because the square-well repulsive potential is used in our simulations.

Each particle interacted with four particles in the same z-level and four particles in different z-levels. Here, N_B is equal to eight, and the interaction energy per particle for the creation of this structure is $4N_B$, provided that a perfectly regular structure without dislocations is formed. However, as shown in Figure 2d, the interaction between particles G and I was broken for

https://doi.org/10.1021/acsomega.3c03624
ACS Omega 2023, 8, 30450−30458

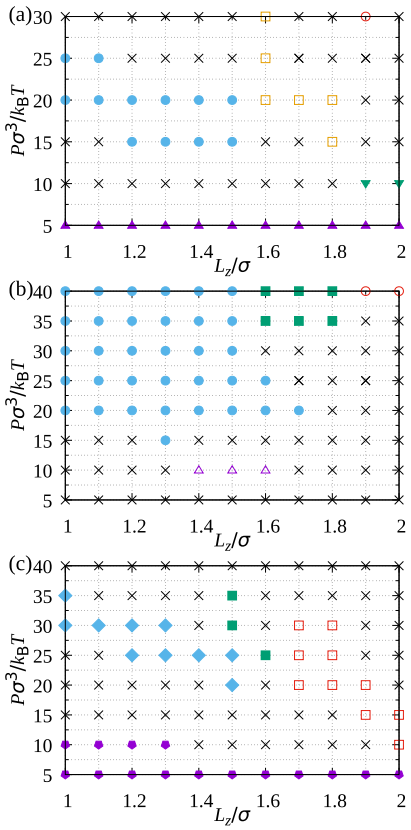

Figure 7. (a) Dependence of typical structure on $P\sigma^3/k_BT$ and L_z/σ for (a) δ = 2.0, (b) δ = 1.6, and (c) δ = 1.3, where solid circle: one-layer hexagonal structure; solid triangle: single-layered string-like structure; solid inverted triangle: double-layer string-like structure; open square: connection of rhombuses; open triangle: honeycomb structure; solid square: double-layer rectangular lattice; open circle: double-layer hexagonal lattice; solid pentagon: low-density single-layer hexagonal structure; solid diamond: single-layer square structure; open square: double-layered square lattice; and cross: disordered (unclassified) structure.

some rhombic tetramers because the distance between them was longer than the distance between other particles.

Double-Layer Hexagonal Structure. When the pressure increased further, the double-layer hexagonal structure, that is, the (111) face of the FCC structure, was created as shown in Figure 1f because the system became compact under high pressure. As shown in Figures 2f and 3iv, each particle in the structure interacted with six adjacent particles in the same z-level, that is, three nearest adjacent particles and three second-nearest adjacent particles in different z-levels. To create this structure, the pressure needs to be high because N_B is large, that is, the repulsive interaction energy is large for the structure. Additionally, the system width must be sufficiently large. For example, for L_z/σ = 1.4 and $P\sigma^3/k_BT$ = 25 (Figures 1e and 2e), because L_z was not sufficiently large to create the double-layer hexagonal lattice, the particles seem to have been packed at random although the pressure was as high as that in Figure 1f.

Detailed Analyses Using Order Parameters for Determining Structures. To quantitatively confirm that the structures expected based on the snapshots are appropriate and to demonstrate the dependence of these structures on L_z/σ and $P\sigma^3/k_BT$, the radial distribution function, average number of interacting particles per particle, the local rotational order, and the structure factor were calculated. The results of radial distribution function were given in Supporting Information, in which it was indicated that the peaks of the radial distribution function agreed with the snapshots (Figure 1). In the followings, the other analyses for the snapshots are shown in Figure 1.

Average Number of Interacting Particles per Particle. First, the average number of interacting particles per particle N_B was calculated.

The distribution of N_B normalized by N is shown in Figure 4. Because the dominant N_B is six (Figure 1a), two (Figure 1b), four (Figure 1c), eight (Figure 1d,e), and approximately 12 (Figure 1d), N_B agrees with the value expected based on Figure 3. Structures with large N_B were created under high pressure because the repulsive interaction increased with N_B.

Local Rotational Order. Second, the local rotational order $\bar{\phi}_m$ was calculated. The definition of $\bar{\phi}_m(i)$ is given by

$$\bar{\phi}_m = \frac{1}{N}\sum_i \phi_m(i) = \frac{1}{N}\sum_i \frac{1}{n_B(i)}\left|\sum_j \exp(im\theta_{ij})\right| \quad (2)$$

In eq 2, $\phi_m(i)$ represents the m-fold local orientational order for the ith particle; $n_B(i)$ is the number of interaction particles for the ith particle; and θ_{ij} is the angle between the x-axis and vector $\boldsymbol{r}_j - \boldsymbol{r}_i$.

A single-layer hexagonal structure was created when L_z was sufficiently small for the system to be considered as a two-dimensional system, such as Figure 1a, or sufficiently large for the system to make a double-layer hexagonal lattice, such as Figure 1f. Therefore, ϕ_6 was investigated as the local rotational order for high-pressure systems. Figure 5 shows how ϕ_6 is distributed in Figure 1a,e,f. For $(L_z/\sigma, P\sigma^3/k_BT)$ = (1.4, 25), and (1.9, 30), ϕ_6 was examined for particles in the same z-level, because the two layers in the structure appeared to be equivalent. Particles with a large ϕ_6 are dominant for $(L_z/\sigma, P\sigma^3/k_BT)$ = (1, 25), and (1.9, 30), which means that a hexagonal structure was created in the systems. For $(L_z/\sigma, P\sigma^3/k_BT)$ = (1.4, 25), particles with large ϕ_6 hardly appear, which agrees with the expectation based on the snapshot Figure 1e.

Structure Factor. In a previous study on a two-dimensional system with large δ,[44] a dodecagonal quasicrystal was created with a pressure higher than the pressure under which the medium-density hexagonal structure was created. Therefore, the structure shown in Figure 1e may be a quasicrystal. Although the system is thin with a finite z width, the differences in the z-coordinate among the particles are small and the structure is considered to resemble a two-dimensional system. Hence, to assess whether the structure is a quasicrystal, the structure factor was calculated and is defined as follows:

$$\boldsymbol{S}(\boldsymbol{q}) = \frac{1}{N}\sum_i\sum_j \exp(2\pi i\boldsymbol{q}\cdot(\boldsymbol{r}_i - \boldsymbol{r}_j)) \quad (3)$$

where $\boldsymbol{q} = (q_x, q_y, 0)$ is the vector parallel to the xy-plane and $\boldsymbol{r}_i$ is the position of the i-th particle.

Figure 6a shows $|\boldsymbol{S}(\boldsymbol{q})|/|\boldsymbol{S}(\boldsymbol{0})|$. Because this structure has several sharp peaks but does not have 12-fold rotational symmetry, the structure is not a dodecagonal quasicrystal structure. For this case, the 12-fold local rotational symmetry ϕ_{12} was also examined (Figure 6b). Particles with large ϕ_{12} were hardly created. Based on the structure factor and

https://doi.org/10.1021/acsomega.3c03624
ACS Omega 2023, 8, 30450−30458

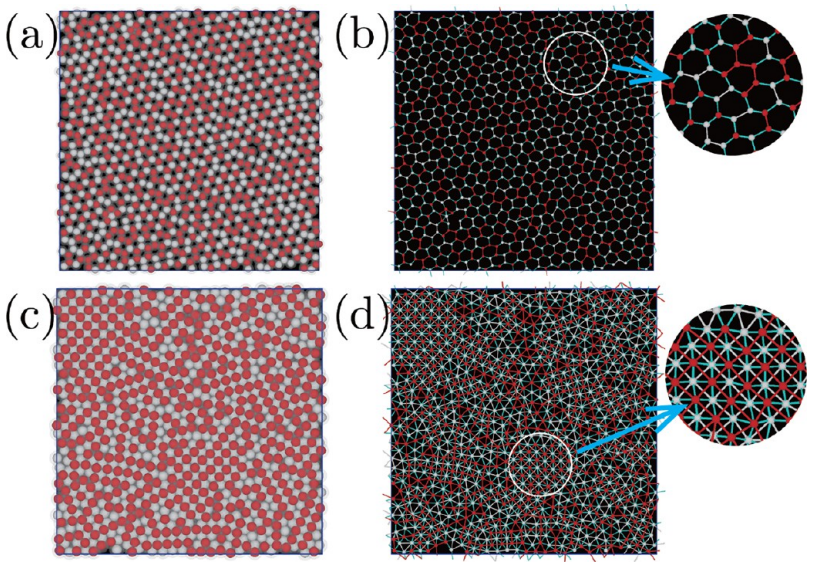

Figure 8. Snapshots viewed from z-direction. δ was set to 1.6 σ; L_z/σ and $P\sigma^3/k_BT$ are (a,b) 1.5 and 10, and (c,d) 1.7 and 35. In (a,c), the particles in $z \geq L_z/2$ and $z < L_z/2$ are indicated by red and white spheres, respectively. In Figure 8b,d, the particles in the z-coordinates are $z \geq L_z/2$ and $z < L_z/2$ and are indicated by small red and white spheres, respectively. The particles with repulsive interaction are connected with red lines when both particles are in $z \geq L_z/2$ and white lines when both particles are both in $z < L_z/2$. When the particles are in different regions, the particles are connected with blue lines. Circular snapshots adjacent to Figure 8b,d are the snapshots zoomed in circular regions.

rotational symmetry, the structure shown in Figure 1e does not exhibit dodecagonal quasicrystal characteristics.

Phase Diagrams. *Phase Diagrams for δ = 2 σ.* After the representative structures were investigated by inspecting the snapshots and calculating several order parameters, the dependence of the created structures on the pressure and system width was determined and is summarized in Figure 7a. The distribution of the z-coordinate of the particles has two peaks of approximately $L_z > 1.6\sigma$. However, regardless of the system thickness, single string-like structure, such as that shown in Figure 1a, was created when the pressure was very low. As the pressure increased, the structure changed to a regular hexagonal structure when L_z was small. In contrast, when L_z was large, a structure was created by the connection of rhombic tetramers and a double-layer string-like structure. When the pressure increased further, a double-layer hexagonal structure was created when L_z was large. Considering that structures with high density are created under large pressure, the formation of the double-layer hexagonal structure under high pressure is reasonable.

In the simulations conducted by this study, a single-layer hexagonal structure changed from an ordered structure to a disorder one, which we cannot classify clearly, as the pressure increased and L_z was small. This change is somewhat strange because a hexagonal structure is expected to be a high-density structure. However, an isothermal−isobaric Monte Carlo simulation conducted by a previous study[43] revealed that a medium-density hexagonal structure changed to a high-density hexagonal structure through the formation of a sigma-phase structure. Accordingly, the transition from a hexagonal structure to a disordered structure is considered to be reasonable because the lattice distance in Figure 1a is larger than σ. In other words, the hexagonal structure shown in Figure 1a is a medium-density hexagonal structure.

The formation of disorder (unclassified) structure instead of sigma phase is probably because the system width is finite. Notably, the high-density hexagonal structure is probably created. Regarding the double-layer hexagonal structure shown in Figure 1f, the structure is a medium-density double-layer hexagonal structure because the lattice constant is larger than unity. In simulations with a higher pressure, the hexagonal structure will change to a disordered structure. If the pressure increases further, a high-density double-layer hexagonal structure will be created.

Phase Diagrams for δ = 1.6 σ and 1.3 σ. In the systems with HCSS potential, the potential width δ affects structures created in two-dimensional cases. Thus, simulations with δ = 1.6 and δ = 1.3 were also conducted and the way in which the dependence of the structure on P and L_z changed with δ was investigated (Figure 8a,b). With the above-mentioned δ values, several structures that were not observed in the system with δ = 2.0 were formed. Figure 7b shows the dependence of the structure for δ = 1.6, and Figure 8 shows the typical structures observed in the system. Figure 8a shows a typical structure, wherein the particles in $z \geq L_z/2$ and $z < L_z/2$ appear at random, even though the difference in the z-coordinates is small. If the difference in the z-coordinates is ignored, the structure can be considered as a honeycomb structure with N_B = 3 (Figure 8b). A string-like structure was not observed. However, considering that a honeycomb structure was also created in the two-dimensional HCSS system, a string-like structure was created with lower pressure in this system and a string-like structure will probably be created when the pressure in this system is much lower. A double-layer rectangular lattice, which is similar to the (001) face of the FCC structure, was created in the high-pressure region when L_z was large (Figure 8c). The difference of the direction of the long side between the upper and lower layers is 90° (Figure 8d). This structure is similar to the buckling structure observed in previous studies.[9−11] The difference between the two structures is attributed to the potential difference. The repulsive interaction damps very fast with the Yukawa potential or is provided by hard-core repulsion. In this simulation, however, the interaction was provided by the square-well repulsion.

https://doi.org/10.1021/acsomega.3c03624
ACS Omega 2023, 8, 30450−30458

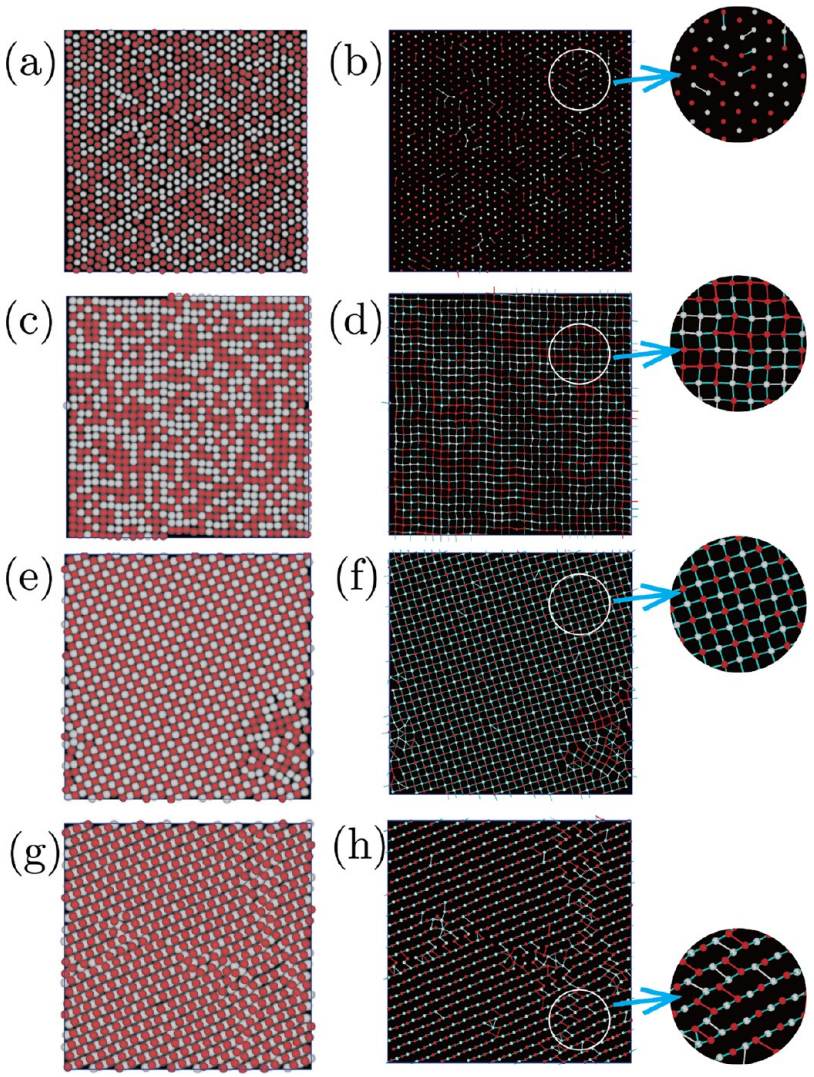

Figure 9. Snapshots of interactions viewed from z-direction for data used in Figure 1. δ is set to 1.3 σ; L_z/σ and $P\sigma^3/k_BT$ are (a,b) 1.1 and 25, (c,d) 1.2 and 5, (e,f) 1.9 and 10, and (g,h) 1.6 and 20. In (a), (c), (e), and (g), the particles in $z \geq L_z/2$ and $z < L_z/2$ are indicated by red and white spheres, respectively. In Figure 9b,d,fh, the particles in the upper half region and lower half region are indicated by small red and white spheres, respectively. The particles with repulsive interaction are connected with red lines when both particles are in $z \geq L_z/2$, white lines when both particles are in $z < L_z/2$, and blue lines when the particles are in different regions. Circular snapshots adjacent to Figure 9b,d are the snapshots zoomed in circular regions.

Figure 7c shows the structure created with $\delta = 1.3$. When the system width was sufficiently small, a single-layer hexagonal structure was created (Figure 9a). The structure is similar to that in Figure 2a, but N_B is different, that is, N_B is six in Figure 2a and zero in Figure 9b. Therefore, the hexagonal structure in Figure 9a is a low-density hexagonal structure. When the pressure increased, a single-layer square lattice was created (Figure 9c). The distance between the particles in the diagonal positions was longer than δ even when the lattice constant decreased by σ. Therefore, N_B is four in the square lattice (Figure 9d). As the system width increased, a double-layer square lattice was also created (Figure 9e). In this structure, the particles in $z \geq L_z/2$ and $z < L_z/2$ appeared alternately and the interaction did not occur between particles in different z-levels because δ was low. The structure resembles the (001) face of the body-centered cubic (BCC) structure. A structure resembling a double-layer oblique structure was also created as shown in Figure 9g. However, from the interaction between particles, it is understood that the structure is actually a string-like structure because the strings were arranged regularly under large pressure.

CONCLUSIONS

This study conducted isothermal−isobaric Monte Carlo simulations to investigate the structures formed by particles interacting with the HCSS potential. The dependence of the structure on the pressure, the system width, and the interaction width is examined, and the formation of various structures was indicated.

The formation of structures, such as single-layer and double-layer hexagonal structures, has also been reported by previous studies that investigated structures created in thin systems.[8−14] Structures such as honeycomb structures and single string-like structures have also been reported in core-corona systems.[43] However, the double-layer string-like structure, which is the structure created by the connection of rhombuses and has a square lattice similar to the (001) face of BCC structure, has not been observed in previous studies. The newly observed

https://doi.org/10.1021/acsomega.3c03624
ACS Omega 2023, 8, 30450−30458

structures are affected both by HCSS potential and the system thinness.

In previous studies for the two-dimensional systems with small δ,[43,44,53] more various structures were created than our simulations with $L_z/\sigma = 1$. One of the reason for the difference is probably that the simulations are performed with higher temperature than the previous studies: several structures may be broken by thermal fluctuations. However, another possibility is that the simulation time is not sufficient and the system did not reach equilibrium cannot be ruled out. For example, some structures which we termed the disordered structures seemed to consist of the mixture of structures. If the long simulations are performed or simulations starts with different initial configurations, these structures may be separated into some phases. The same is true for the formation of quasicrystal structures. Although quasicrystal structures were observed in HCSS systems in previous studies,[41−44] these structures were not observed in the simulations conducted in this study. There is a possibility that the formation of quasi structures was prevented by the finite system width L_z, but quasicrystal structures may be created in the parameter region with disordered structures if we perform simulations more carefully. For example, the simulations should be performed longer, how to change the particle positions and the system volume should be changed, or different initial conditions should be used to confirm whether quasicrystals are created. Hence, the task of future work will be to carry out more careful simulations and detailed analyses on the disordered structures.

■ ASSOCIATED CONTENT

Supporting Information

The Supporting Information is available free of charge at https://pubs.acs.org/doi/10.1021/acsomega.3c03624.

Figure S1: Radial distribution function $g(r)$ for snapshots in Figure 1, where Δr is set to 10^{-2}; L_z/σ and $P\sigma^3/k_BT$ are (a)1 and 25, (b)1.2 and 5, (c)1.9 and 10, (d)1.6 and 20, (e)1.4 and 25, and (f)1.9 and 30, and Figure S2: Radial distribution function $g(r)$ for snapshots in Figure 1, where the contributions from the particles in the same z-level and those in different z-levels are indicated, respectively. L_z/σ and $P\sigma^3/k_BT$ are (a)1.9 and 10, (b)1.6 and 20, (c)1.4 and 25, and (d)1.9 and 30 (PDF)

■ AUTHOR INFORMATION

Corresponding Author

Masahide Sato − *Emerging Media Initiative, Kanazawa University, 920-1192 Kanazawa, Japan;* orcid.org/0000-0001-8298-9016; Email: msato002@staff.kanazawa-u.ac.jp

Author

Ryo Muragishi − *Graduate School of Natural Science and Technology, Kanazawa University, 920-1192 Kanazawa, Japan*

Complete contact information is available at: https://pubs.acs.org/10.1021/acsomega.3c03624

Notes

The authors declare no competing financial interest.

■ ACKNOWLEDGMENTS

This study was supported by JSPS KAKENHI (Grant nos. JP20K03782, JP21K04908, and 23k03258) and the Grant for Joint Research Program of the Institute of Low Temperature Science, Hokkaido University (Grant nos. 22G015 and 23G028). The authors thank Edanz (https://jp.edanz.com/ac) for editing a draft of this manuscript.

■ REFERENCES

(1) Algara-Siller, G.; Lehtinen, O.; Wang, F. C.; Nair, R. R.; Kaiser, U.; Wu, H. A.; Geim, A. K.; Grigorieva, I. V. Square ice in graphene nanocapillaries. *Nature* **2015**, *519*, 443.

(2) Oğuz, E. C.; Messina, R.; Löwen, H. Helicity in cylindrically confined Yukawa systems. *Europhys. Lett.* **2011**, *94*, 28005.

(3) Wu, G.; Cho, H.; Wood, D. A.; Dinsmore, A. D.; Yang, S. Confined Assemblies of Colloidal Particles with Soft Repulsive Interactions. *J. Am. Chem. Soc.* **2017**, *139*, 5095−5101.

(4) Ma, P.; Chan, H.-K. Densest-Packed Columnar Structures of Hard Spheres: An Investigation of the Structural Dependence of Electrical Conductivity. *Front. Phys.* **2021**, *9*, No. 778001.

(5) Pieranski, P. Two-Dimensional Interfacial Colloidal Crystals. *Phys. Rev. Lett.* **1980**, *45*, 569.

(6) Pieranski, P.; Strzelecki, L.; Pansu, B. Thin Colloidal Crystals. *Phys. Rev. Lett.* **1983**, *50*, 900−903.

(7) Neser, S.; Bechinger, C.; Leiderer, P.; Palberg, T. Finite-Size Effects on the Closest Packing of Hard Spheres. *Phys. Rev. Lett.* **1997**, *79*, 2348−2351.

(8) Schmidt, M.; Löwen, H. Phase diagram of hard spheres confined between two parallel plates. *Phys. Rev. E* **1997**, *55*, 7228−7241.

(9) Fortini, A.; Dijkstra, M. Phase behaviour of hard spheres confined between parallel hard plates: manipulation of colloidal crystal structures by confinement. *J. Phys.: Condens. Matter* **2006**, *18*, L371−L378.

(10) Ramiro-Manzano, F.; Meseguer, F.; Bonet, E.; Rodriguez, I. Faceting and Commensurability in Crystal Structures of Colloidal Thin Films. *Phys. Rev. Lett.* **2006**, *97*, No. 028304.

(11) Ramiro-Manzano, F.; Bonet, E.; Rodriguez, I.; Meseguer, F. Layering transitions in confined colloidal crystals: The hcp-like phase. *Phys. Rev. E* **2007**, *76*, No. 050401(R).

(12) Kaneko, T.; Mima, T.; Yasuoka, K. Phase diagram of Lennard-Jones fluid confined in slit pores. *Chem. Phys. Lett.* **2010**, *490*, 165.

(13) Curk, T.; de Hoogh, A.; Martinez-Veracoechea, F. J.; Eiser, E.; Frenkel, D.; Dobnikar, J.; Leunissen, M. E. Layering, freezing, and re-entrant melting of hard spheres in soft confinement. *Phys. Rev. E* **2012**, *85*, No. 021502.

(14) Oğuz, E. C.; Reinmüller, A.; Schöpe, H. J.; Palberg, T.; Messina, R.; Löwen, H. Crystalline multilayers of charged colloids in soft confinement: experiment versus theory. *J. Phys.: Condens. Matter* **2012**, *24*, No. 464123.

(15) Oğuz, E. C.; Marechal, M.; Ramiro-Manzano, F.; Rodriguez, I.; Messina, R.; Meseguer, F. J.; Löwen, H. Packing Confined Hard Spheres Denser with Adaptive Prism Phases. *Phys. Rev. Lett.* **2012**, *109*, No. 218301.

(16) Antlanger, M.; Doppelbauer, G.; Mazars, M.; Kahl, G. Crystal phases of soft spheres systems in a slab geometry. *J. Chem. Phys.* **2014**, *140*, No. 044507.

(17) Harth, K.; Mauney, A.; Stannarius, R. Frustrated packing of spheres in a flat container under symmetry-breaking bias. *Phys. Rev. E* **2015**, *91*, No. 030201(R).

(18) Iwashita, Y.; Kimura, Y. Spatial confinement governs orientational order in patchy particles. *Sci. Rep.* **2016**, *6*, 27599.

(19) Deißenbeck, F.; Löwen, H.; Oğuz, E. C. Ground state of dipolar hard spheres confined in channels. *Phys. Rev. E* **2018**, *97*, No. 052608.

(20) Fomin, Y. D. Between two and three dimensions: Crystal structures in a slit pore. *J. Colloid Interface Sci.* **2020**, *580*, 135−145.

(21) Sato, M. Effect of patch area and interaction length on clusters and structures formed by one-patch particles in thin systems. *ACS Omega* **2020**, *5*, 28812−28822.

(22) Villada-Balbuena, A.; Jung, G.; Zuccolotto-Bernez, A. B.; Franosch, T.; Egelhaa, S. U. Layering and packing in confined colloidal suspensions. *Soft Matter* **2022**, *18*, 4699−4714.
(23) Bock, H.; Gubbins, K. E.; Ayappa, K. G. Solid/solid phase transitions in confined thin films: A zero temperature approach. *J. Chem. Phys.* **2005**, *122*, No. 094709.
(24) de Nijs, B.; Dussi, S.; Smallenburg, F.; Meeldijk, J. D.; Groenendijk, D. J.; Filion, L.; Imhof, A.; van Blaaderen, A.; Dijkstra, M. Entropy-driven formation of large icosahedral colloidal clusters by spherical confinement. *Nat. Mater.* **2015**, *14*, 56−60.
(25) Chen, Y.; Yao, Z.; Tang, S.; Tong, H.; Yanagishima, T.; Tanaka, H.; Tan, P. Morphology selection kinetics of crystallization in a sphere. *Nat. Phys.* **2021**, *17*, 121−127.
(26) Wang, D.; Hermes, M.; Kotni, R.; Wu, Y.; Tasios, N.; Liu, Y.; de Nijs, B.; van der Wee, E. B.; Murray, C. B.; Dijkstra, M.; van Blaaderen, A. Interplay between spherical confinement and particle shape on the self-assembly of rounded cubes. *Nat. Commun.* **2018**, *9*, 2228.
(27) Wang, D.; Hermes, M.; Najmr, S.; Tasios, N.; Grau-Carbonell, A.; Liu, Y.; Bals, S.; Dijkstra, M.; Murray, C. B.; van Blaaderen, A. Structural diversity in three-dimensional self-assembly of nanoplatelets. by spherical confinement. *Nat. Commun.* **2022**, *13*, 6001.
(28) Wang, D.; Dasgupta, T.; van der Wee, E. B.; Zanaga, D.; Altantzis, T.; Wu, Y.; Coli, G. M.; Murray, C. B.; Bals, S.; Dijkstra, M.; van Blaaderen, A. Binary icosahedral clusters of hard spheres in spherical confinement. *Nat. Phys.* **2021**, *17*, 128−134.
(29) Zhu, G.; Gao, L.; Xu, Z.; Dai, X.; Zhang, X.; Yan, L.-T. Entropy-Driven Unconventional Crystallization of Spherical Colloidal Nanocrystals Confined in Wide Cylinder. *Nano Lett.* **2021**, *21*, 8439−8446.
(30) Sato, M. Clusters formed by dumbbell-like one-patch particles confined in thin systems. *Sci. Rep.* **2021**, *11*, 18078.
(31) Bautista-Carbajal, G.; Gurin, P.; Varga, S.; Odriozola, G. Phase diagram of hard squares in slit confinement. *Sci. Rep.* **2018**, *8*, 8886.
(32) Constantin, D.; Pansu, B.; Impèror, M.; Davidson, P.; Ribot, F. Repulsion Between Inorganic Particles Inserted Within Surfactant Bilayers. *Phys. Rev. Lett.* **2008**, *101*, No. 098101.
(33) Pansu, B.; Lecchi, A.; Constantin, D.; Impéror-Clerc, M.; Veber, M.; Dozov, I. Insertion of Gold Nanoparticles in Fluid Mesophases: Size Filtering and Control of Interactions. *J. Phys. Chem. C* **2011**, *115*, 17682−17687.
(34) Weis, J-J.; Kahn, M.; Kahl, G. Ordered equilibrium structures of soft particles in thin layers. *J. Chem. Phys.* **2010**, *133*, 224504.
(35) Gribova, N.; Arnold, A.; Schilling, T.; Holm, C. How close to two dimensions does a Lennard-Jones system need to be to produce a hexatic phase? *J. Chem. Phys.* **2011**, *135*, No. 054514.
(36) Young, D. A.; Alder, B. J. Melting-Curve Extrema from a Repulsive "Step" Potential. *Phys. Rev. Lett.* **1997**, *38*, 1213−1216.
(37) Malescio, G.; Pellicane, G. Stripe phases from isotropic repulsive interactions. *Nat. Mater.* **2003**, *2*, 97−100.
(38) Malescio, G.; Pellicane, G. Stripe patterns in two-dimensional systems with core-corona molecular architecture. *Phys. Rev. E* **2004**, *70*, No. 021202.
(39) Glaser, M. A.; Grason, G. M.; Kamien, R. D.; Kŏsmrlj, A.; Santangelo, C. D.; Ziherl, P. Soft Spheres Make More Mesophases. *Europhys. Lett.* **2007**, *78*, 46004.
(40) Norizoe, Y.; Kawakatsu, T. Particle Monte Carlo simulation of stringlike colloidal assembly in two and three dimensions. *J. Chem. Phys.* **2012**, *137*, No. 024904.
(41) Dotere, T.; Oshiro, T.; Ziherl, P. Mosaic two-lengthscale quasicrystals. *Nature* **2014**, *506*, 208−211.
(42) Pattabhiramana, H.; Gantapara, A. P.; Dijkstra, M. On the stability of a quasicrystal and its crystalline approximant in a system of hard disks with a soft corona. *J. Chem. Phys.* **2015**, *143*, 164905.
(43) Pattabhiramana, H.; Dijkstra, M. On the formation of stripe, sigma, and honeycomb phases in a core-corona system. *Soft Matter* **2017**, *13*, 4418.
(44) Pattabhiramana, H.; Dijkstra, M. Phase behaviour of quasicrystal forming systems of core-corona particles. *J. Chem. Phys.* **2017**, *146*, 114901.
(45) Rey, M.; Fernandez-Rodriguez, M. A.; Steinacher, M.; Scheidegger, L.; Geisel, K.; Richtering, W.; Squires, T. M.; Isa, L. Isostructural solid-solid phase transition in monolayers of soft core-shell particles at fluid interfaces: structure and mechanics. *Soft Matter* **2016**, *12*, 3545.
(46) Geisel, K.; Isa, L.; Richtering, W. The Compressibility of pH-Sensitive Microgels at the Oil-Water Interface: Higher Charge Leads to Less Repulsion. *Angew. Chem., Int. Ed.* **2014**, *53*, 4905.
(47) Vogel, N.; Fernández-López, C.; Perez-Juste, J.; Liz-Marzan, L. M.; Landfester, K.; Weiss, C. K. Ordered Arrays of Gold Nanostructures from Interfacially Assembled Au@PNIPAM Hybrid Nanoparticles. *Langmuir* **2012**, *28*, 8985.
(48) Rey, M.; Law, A. D.; Buzza, D. M. A.; Vogel, N. Anisotropic Self-Assembly from Isotropic Colloidal Building Blocks. *J. Am. Chem. Soc.* **2017**, *139*, 17464.
(49) Rey, M.; Yu, T.; Bley, K.; Landfester, K.; Buzza, D. M. A.; Vogel, N. Amphiphile-Induced Anisotropic Colloidal Self-Assembly. *Langmuir* **2018**, *34*, 9990.
(50) El-Tawargy, A. S.; Stock, D.; Gallei, M.; Ramadan, W. A.; Shams El-Din, M. A.; Reiter, G.; Reiter, R. Multiple Structural Transitions in Langmuir Monolayers of Charged Soft-Shell Nanoparticles. *Langmuir* **2018**, *34*, 3909.
(51) Fischer, S.; Exner, A.; Zielske, K.; Förster, S. Colloidal quasicrystals with 12-fold and 18-fold diffraction symmetry. *Proc. Natl. Acad. Sci. U. S. A.* **2011**, *108*, 1810−1814.
(52) Fonseca, E. R.; Mendoza, C. I. Self-assembly of core-corona particles confined in a circular box. *J. Phys.: Condens. Matter* **2020**, *32*, No. 015101.
(53) Somerville, W. R. C.; Law, A. D.; Rey, M.; Vogel, N.; Archer, A. J.; Buzza, D. M. A. Pattern formation in two-dimensional hard-core/soft-shell systems with variable soft shell profiles. *Soft Matter* **2020**, *16*, 3564−3573.

https://doi.org/10.1021/acsomega.3c03624
ACS Omega 2023, 8, 30450−30458